IMU-aided detection and mitigation of Human Body Shadowing for UWB positioning

1st Cedric De Cock
Dept. of Information Technology
imec-WAVES, Ghent University
Ghent, Belgium
cedric.decock@ugent.be

2rd Sander Coene
Dept. of Information Technology
imec-WAVES, Ghent University
Ghent, Belgium
sander.coene@ugent.be

3rd Ben Van Herbruggen
Dept. of Information Technology
imec, IDLab, Ghent University
Ghent, Belgium
ben.vanherbruggen@ugent.be

2nd Luc Martens
Dept. of Information Technology
imec-WAVES, Ghent University
Ghent, Belgium
luc.martens@ugent.be

4nd Wout Joseph
Dept. of Information Technology
imec-WAVES/Ghent University
Ghent, Belgium
wout.joseph@ugent.be

5th David Plets
Dept. of Information Technology
imec-WAVES/Ghent University
Ghent, Belgium
david.plets@ugent.be

Abstract—**Ultra-wideband (UWB) indoor positioning systems have the potential to achieve decimeter-level accuracy. However, the performance can degrade significantly under Non-Line-of-Sight (NLoS) conditions. Detection and mitigation of NLoS conditions is a complex problem, and has been the subject of many works over the past decades. When localizing pedestrians, human body shadowing (HBS) is an important cause of NLoS. In this paper, we propose an HBS mitigation strategy based on the orientation of the body and tag relative to the UWB anchors by attaching an inertial measurement unit to the UWB tag. Two algorithms are designed and implemented, of which the second algorithm is designed for robustness against errors in the IMU's estimated heading. The proposed algorithms are validated by UWB Two Way Ranging (TWR) measurements, performed in two environments. Two more algorithms are implemented as a benchmark, of which one is based on the estimated first path power, and the other is based on range residuals. The proposed algorithm outperforms the other algorithms in the higher error statistics, achieving a 49% reduction of the p90 error depending on the environment.**

Index Terms—**UWB, ToF, indoor localization, human body shadowing, inertial measurement unit, Non-Line-of-Sight**

I. INTRODUCTION

In Time-of-Flight (ToF) ranging, the travel time of a signal is measured to estimate the distance between a tag and anchor [1]. UWB ranging has several advantages over other technologies, i.e. centimeter-level accuracy, immunity to multipath fading and low power consumption [1]. Commercial Off-the Shelf (COTS) UWB transceivers have been available for several years, of which the Decawave DW1000 has shown to be the best performing [2].

While high ranging accuracy can be achieved in line-of-sight (LOS), there is still ongoing research in mitigating the effects of non-line-of-sight (NLoS) conditions. In these conditions, the direct path between the tag and an anchor is (partly) obstructed by a wall, object, or the human body. Depending on the obstruction, it is possible that the received power along the direct path is too low, and through reflection or diffraction

an indirect path component of the signal is detected instead. Because the indirect path covers a larger distance than the direct unobstructed path, the signal is detected with a delay causing a positive bias on the range estimation [3]. Human body shadowing (HBS) is a specific NLoS condition and plays a large role in pedestrian tracking with on-body tags. The effects of HBS on UWB ranging has been investigated in other works [4]–[6], which have shown that the impact is heavily dependent on the body-tag orientation to the anchor as well as the placement of the tag on the body. However, most works on UWB NLoS detection/mitigation offer solutions for NLoS in general [3], [7]–[12]. While some works do differentiate between NLoS caused by the human body and the environment (e.g. walls) [3], [13], they do not use the insight on the extent of HBS, which the tag-body orientation can provide. Furthermore, many NLoS mitigation methods are based on extracting information from the Channel Impulse Response (CIR). However, extracting the CIR from a COTS transceiver such as the DW1000, is time consuming and (depending on the desired resolution) not feasible for real-time applications [14].

Some recent works focus on hybrid systems, which fuse (UWB) ranging with an Inertial Navigation System (INS) or Pedestrian Dead Reckoning (PDR) [15], [16]. INS and PDR use an inertial measurement unit (IMU) to estimate the pedestrian's movement (by e.g. detecting steps), and enable infrastructure-less localization [17]. While having their own drawbacks, INS/PDR's immunity to NLoS can therefore reduce NLoS errors in a hybrid positioning system.

In this paper, it is hypothesized that an IMU can also be used to detect and compensate HBS, based on the tag-body-anchor orientation. Two IMU-based HBS mitigation approaches are implemented on top of an existing positioning algorithm, and evaluated with measurements using COTS hardware in two environments.

The contributions of this paper are as follows:

1) Two IMU-based human body shadowing detection and mitigation methods for UWB-IPS are presented.
2) Experimental validation of the proposed method by low-frequency static UWB Channel Impulse Response (CIR) measurements and ranging, and with high-frequency dynamic UWB ranging, both in human body NLoS conditions and with IMU measurements.

The remainder of the paper consists of an overview of related works (section II), the measurement methodology and implemented algorithms (section III), evaluation of the results (section IV), and the conclusions and future work (section V).

II. RELATED WORKS

Figure 1 explains the configuration considered here and in related work. $\phi \in [0°, 180°]$ is the incident angle of the signal in the horizontal plane relative to the body orientation of the user. More specifically, it is the smallest angle between vectors $\overrightarrow{PT}$ and $\overrightarrow{TA}$, where T, P and A are the 2D positions of the tag, person, and anchor respectively (Figure 1). The tag is carried in front of the body during our measurements, as depicted in Figure 1. For $\phi \in [90°, 180°]$, there is some degree of body obstruction between the tag and the anchor.
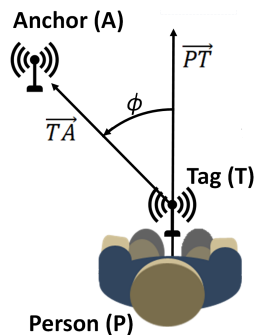

Fig. 1: Tag-anchor configuration and symbols used in this paper

1) Human body influence on UWB ranging: UWB measurements in anechoic chambers with several antennas show that the received power is not significantly affected by the human body for $\phi < 150°$ [18]. Very large attenuations for $\phi > 180°$ are observed in [19]. Indoor and outdoor ranging experiments were performed with the Decawave TREK1000 development kits in [5], along with simulations. It was found that the signal is largely unaffected for $\phi < 67.5°$, while the ranging error increases from 20 cm to 30 cm for $67.5° < \phi < 112°$ in the simulations. However, the average error increases up to 60 cm for $180° > \phi > 112°$. Similarly, [20] reports no significant influence on ranging compared to pure LOS ranging for $\phi < 90°$ with the tag held in front of the body, but large errors occured above $150°$. The difference in reported angle intervals can be attributed to the distance between body and tag, as [5] found a 3 dB rise in the electric field by placing the tag only a few cm away from the body. For larger ϕ, reflected signals become dominant over creeping

waves. It is noticed in [21] that weak reflections from the absorber blocks of the anechoic chamber can be stronger than the creeping waves for full NLOS. A 90th percentile range error of 4 m in NLOS conditions due to reflections is reported in [4]. Based on measurements with an on-body tag in a realistic environment, [12] concludes that HBS has the highest impact on ranging accuracy.

The influence of tag placement on range error and packet loss are investigated in [4] and [6] respectively. Both works conclude that the head (quasi LOS) is the best place and the chest/stomach is the worst place for the tag. Furthermore, the error increase for large ϕ values also depends on the TOF estimation algorithm itself, e.g. leading-edge detection (LDE) is more susceptible to HBS than the SAGE algorithm [22]. Lastly, [4] proposes adaptive noise models for on-body UWB ranging depending on the tag placement and ϕ. [13], [20] use similar models for tags in front of the body at chest height.

2) Detection and mitigation of HBS in UWB ranging: NLoS detection and mitigation have been researched extensively during the past decades, but few works try to mitigate HBS specifically [3], [4], [6], [20]. [3] uses a fuzzy classifier to detect HBS or (a combination of) other types of NLoS, and mitigates the ranging errors accordingly before calculating the position. NLoS including HBS is detected by thresholding the relative first path power with 93% accuracy in [12], which then uses a polynomial function to estimate the range error. The corrected ranges are then used on several positioning algorithms, of which the EKF performed best in severe NLoS conditions. Instead of mitigating the range errors before calculating the position, the first path power is used directly in [6] to estimate the noise variance of an EKF and Particle Filter (PF), but with mixed results. Similarly, an Extended Kalman Filter (EKF) is used in [4], for which the measurement noise variance depends on the placement of the tag, e.g. low variance on the head, high variance on the chest.

A PF with adaptive noise model is proposed in [20], where ϕ is estimated based on the heading provided by a gyroscope and the PF's estimated position. If ϕ is larger than a predefined threshold, the channel is considered NLOS and a Gamma distribution is used. Otherwise the channel is LOS and a Gaussian distribution is used. The same approach is used in [23], but the orientation is based on the walking direction estimated from past estimated positions.

However, the PFs in [20], [23] require a fixed angle between the walking direction and vector $\overrightarrow{PT}$ (i.e. sideways/backwards walking is not allowed). They also use knowledge of range error statistics which varies depending on the environment and tag position on the body. We propose an HBS mitigation algorithm based on an IMU, which does not rely on error statistics and does not require a fixed angle between the walking direction and $\overrightarrow{PT}$.

TABLE I: UWB hardware and measurement settings

Tag position	abdomen
UWB Channel	5
Pulse Repetition Frequency (MHz)	64
Bitrate (kb/s)	850
Preamble length (# bytes)	1024

III. METHOD

A. Measurement configurations

1) Environments: For designing and testing the positioning algorithms, measurements are performed in two environments. One is an 11 m x 9 m open environment with eight UWB anchors in the Industrial Internet of Things (IIoT) lab. This lab has no obstacles other than the person carrying the tag. The other environment is a 41 m x 27 m office with six UWB anchors (OfficeLab). The anchors in IIoT lab are placed in two groups in the corners of the lab as shown in Figure 2a. The lower four anchors are placed at a height of $0.4m$, the higher four are placed at $2.6m$. The IIoT lab also has a Qualisys motion capture (mocap) system with seven infrared (IR) cameras, providing ground truth with millimeter-level accuracy. However, mocap accuracy degrades towards the edge of the lab environment, thus the measurement area is confined to a 6.3 m x 4.4 m area, marked by the dashed red lines in Figure 2a.

The office has six anchors as shown on the floorplan in Figure 2c, which includes the material type of each wall. The upper corridor and the rooms above it are mostly separated by drywwalls. All anchors are placed close to the ceiling around 2.60 m above ground level, and their location is known with cm-level accuracy. The building area is 41 m x 27 m, but the measurement area is confined to the upper horizontal corridor in Figure 2c.

2) Data collection: We used the Open Source UWB hardware platform "Wi-Pos" [24], which consists of a Decawave DW1000 UWB transceiver (IEEE 802.15.4a), an external planar dipole antenna attached to the UWB transceiver's SMA connector, and a Zolertia RE-Mote. The latter is an IoT platform with a CC1200 sub-GHz radio (IEEE 802.15 g), which manages a symmetrical double-sided two-way UWB ranging scheme using a custom Time Division Multiple Access protocol [25]. The tag output is read from the tag's USB serial port and consists of the CIR and estimated range at a rate of 1 Hz, or only the range at 24 Hz. The CIR is not required for the technique proposed here, but it is useful for other/future research. Therefore, 24 Hz range measurements are performed during the dynamic tests, while 1 Hz CIR and range measurements are performed during the static tests. The UWB hardware settings are provided in Table I.

IR markers are placed on the tag, which allows the mocap system to provide accurate position and orientation of the tag at a sampling rate of 90 Hz. However, the human body also causes shadowing when tracking the UWB tag
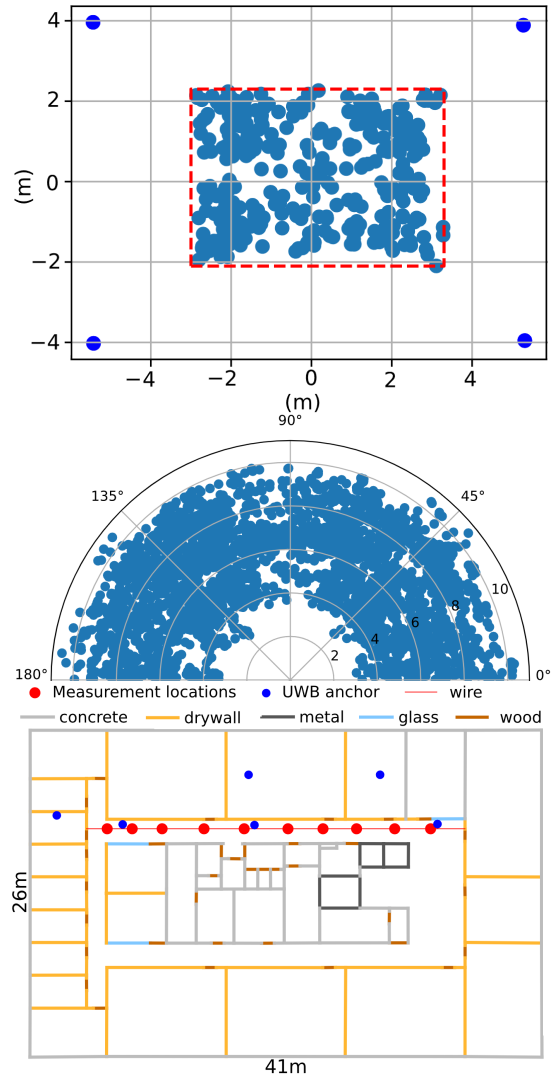

Fig. 2: The measurement area in the IIoT lab is marked by the red dashed rectangle in (a), and includes 390 measurements positions in a variety of orientations. The dots in the corners represent the UWB anchors. (b) shows a scatterplot of the true distance and incident angle ϕ measured by the mocap system for each tag-anchor link, at each measurement position. The floorplan of the office lab is shown in (c), where the blue and red dots represent the UWB anchors and measurement locations respectively. The latter are marked on the floor below a wire (red line).

with mocap. Therefore, all hardware is taped onto a piece of cardboard and markers are put on the sides as shown in Figure 3. The tag is positioned at the abdomen, where the markers stick out to the sides of the body, so they are still in view of enough cameras in case the tag itself is not. The local coordinate system is defined with the antenna as the origin, the Z-axis pointing up and the Y-axis perpendicular to the antenna surface, i.e. $\overrightarrow{PT}$. Furthermore, a Raspberry Pi (RPi) is used to read the tag output and the sensor data of
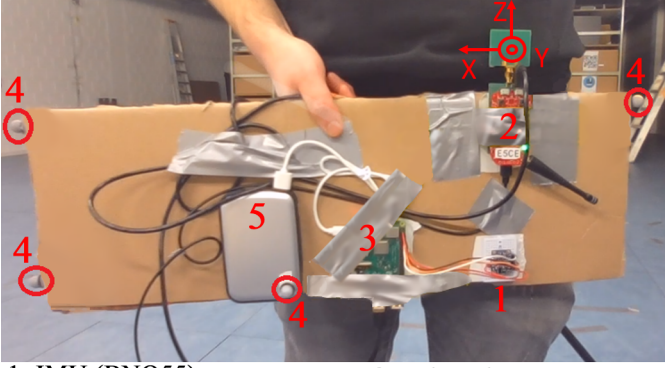
1: IMU (BNO55)
2: UWB tag (Wi-PoS)
3: Raspberry Pi
4: Infrared marker
5: power bank

Fig. 3: Picture of the measurement setup. A Raspberry Pi reads the data from the UWB tag (Wi-Pos) and the IMU (BNO55). Infrared markers on the side of the cardboard allow consistent and accurate ground truth by motion capture.

the Adafruit BNo55 IMU.

In the IIoT lab, the mocap, UWB tag and IMU output are published to an MQTT broker, where a subscriber receives all data synchronized and timestamped. During the measurements, the pedestrian walks around in the measurement area. Every other step, the pedestrian stands still for at least eight seconds. The average position and orientation measured by mocap while standing still defines the ground truth. This results in 390 positions scattered across the measurement area as shown in Figure 2a. The tag was pointed in different directions, so all ϕ values are well represented for ranges between 3 m and 10 m, as shown on the scatterplot in Figure 2b. There is no mocap system in Officelab, making accurate ground truth difficult to attain, and each measurement position has to be defined manually. Therefore, the experiment area is limited to the upper corridor in Figure 2c, where a wire is attached to the frame of two doors on opposite sides of the corridor. Right below the wire, ten measurement positions are marked. Measurements are performed at each position in four orientations (along the cardinal directions), resulting in 40 unique configurations.

B. Assessment of human body orientation effect on ranging

Assessment of HBS effects on UWB ranging and positioning is based on the horizontal incident angle $\phi \in [0°, 180°]$ between the direct tag-anchor path and the direction the tag is pointed at, as described in section II. This angle is estimated with eq. (1), where T is an initial estimate of the tag position and h_{imu} is the tag heading provided by the IMU.

$$\phi_{est} = acos(\frac{[cos(h_{imu}), sin(h_{imu})] \cdot \overrightarrow{TA}}{|\overrightarrow{TA}|}) \quad (1)$$

When ϕ is known, a new position can be calculated where the range from a tag-anchor link with a value of ϕ higher than an HBS threshold ϕ_{HBS} is ignored (i.e. anchor selection)

or its contribution to the positioning is reduced. Since eq. (1) requires an estimated position, its accuracy and thus the effectiveness of the HBS mitigation strategy are highly dependent on the positioning algorithm itself (see section IV).

C. Linearized Least Squares positioning

As discussed in section III-B, eq. (1) requires an estimated position for HBS assessment. In this paper, we use the Linearized Least Squares (LLS) multilateration algorithm as a basis for our HBS assessment, which is then used to estimate a new and more accurate position. The solution for (Weighted) LLS multilateration with n anchors is explained in [26] and is calculated with eq. (2).

$$\mathbf{x} = (A^T A)^{-1} A^T \mathbf{b} \quad (2)$$

x is a vector of which the last two elements represent the 2D position.

$$A = \begin{bmatrix} 1 & -2x_1 & -2y_1 \\ 1 & -2x_2 & -2y_2 \\ & \vdots & \\ 1 & -2x_n & -2y_n \end{bmatrix}, \mathbf{b} = \begin{bmatrix} s_1^2 - x_1^2 - y_1^2 \\ s_2^2 - x_2^2 - y_2^2 \\ \vdots \\ s_n^2 - x_n^2 - y_n^2 \end{bmatrix} \quad (3)$$

s_i is the measured 2D distance between the tag and anchor i with position $\mathbf{x}_{anc}^i = (x_i, y_i, z_i)$. Note that eq. (3) differs slightly from [26], because the latter provides the 3D solution. Since the experiments are performed in 3D space, each measured (3D) range r_i is converted with eq. (4).

$$s_i^2 = r_i^2 - (z_i - z_{tag})^2 \quad (4)$$

The tag height z_{tag} is considered a known constant.

D. Mitigation of human body shadowing effects

The HBS mitigation strategy employed in this paper is based on discarding the range measurements with high likeliness of large errors, i.e anchor selection (AS). This strategy has been used as a NLoS mitigation strategy for many years [27], and is still being used in recent literature [28].
A simple AS algorithm (Algorithm 1) is proposed first. An initial position is calculated using n ranges, where n is the amount of anchors. With this position and the tag heading h_{imu}, the azimuth ϕ_i with $i \in [0, n-1]$, can be determined for each ith tag-anchor link (eq. 1). Starting from the highest value of ϕ, corresponding ranges are discarded as long as more than three ranges, or no ranges with $\phi > \phi_{HBS}$ remain. The final position is then estimated, again with eq. (2), but only using the non-discarded ranges. This AS algorithm is labeled 'LLS-ASϕ_{imu}'. Instead of ϕ, the relative signal strength of the first path component FP can also be used to assess HBS influence. In fact, it is used in several works to detect HBS [6], [29], and NLOS conditions in general [12], [14]. FP is defined as the difference between the estimated received signal strength and the strength of its first path component, and can be calculated directly from metadata produced by the DW1000 transceiver. Since FP is frequently used for NLoS detection in recent literature involving COTS UWB hardware,

we also test Algorithm 1 using FP to assess the HBS effect. This algorithm is labeled as 'LLS-AS_FP', and is used as a benchmark. Note that the first step of Algorithm 1 is not necessary for LLS-AS_FP. The last variation of Algorithm 1 is labeled as 'LLS-ASϕ_{mocap}', which uses the ground truth position and orientation to calculate ϕ. Knowledge of the exact ϕ value provides insight on the maximum achievable performance of this orientation-based AS method, as well as the influence of position and/or heading errors on the assessment and subsequently on the mitigation of HBS.

Algorithm 1

Data: n ranges with known anchor positions, tag heading h_{imu}, HBS threshold ϕ_{HBS}
Result: 2D tag position

1: $\mathbf{x}_{tag}^{init} \leftarrow (2);$ ▷ use all available links
2: $\phi \leftarrow (1);$ ▷ based on rough position and h_{imu}
3: sort ϕ descending;
4: **while** length(ϕ) > 3 **do**
5:     **if** $\phi[0] > \phi_{HBS}$ **then**
6:        ϕ.pop(0);
7:     **else**
8:        break;
9:     **end if**
10: **end while**
11: $\mathbf{x}_{tag} \leftarrow (2);$ ▷ use links corresponding to ϕ

Algorithm 1 has some disadvantages though: first, it depends on the initial unmitigated position for calculating ϕ. If ϕ_{true} is close to ϕ_{HBS}, errors in the unmitigated position and/or estimated heading can cause a 'bad' range to be used and/or a 'good' range to be excluded. There is also a possibility that the range error is small (section IV-A) and is still usable, even when HBS is correctly detected and as a consequence, the range is discarded.

Therefore, Algorithm 2 is proposed. First, a candidate position is calculated for all $\sum_{k=3}^{n} \binom{n}{k}$ anchor subsets. A weight w^j is then calculated for each jth candidate position with eq. (5), where ϕ_i^j is the azimuth of the ith link, S^j is the subset of links, and $\mathcal{L}(...)$ is a likelihood function.

$$w^j = \prod_{i=0}^{n-1} \begin{cases} \mathcal{L}(\phi_i^j | \overline{HBS}) & i \in S^j \\ \mathcal{L}(\phi_i^j | HBS) & i \notin S^j \end{cases} \quad (5)$$

The likelihood functions are Gaussian Cumulative Distribution Functions (CDFs) centered around a threshold ϕ_{HBS}, as shown in Figure 4. Eq. (5) uses the assumption that the links in a given subset, which are used to calculate a candidate position, are not under HBS influence, i.e $\overline{HBS}$. If a tag-anchor link i is not under influence of HBS, then $\phi_i < \phi_{HBS}$ and vice versa. Therefore, if $i \in S^j$ and ϕ_i^j is low/high, then its likelihood is high/low respectively. A link with ϕ close to the threshold has a balanced likelihood regardless of its inclusion in the subset. These smooth likeliness functions make the positioning algorithm robust against heading errors
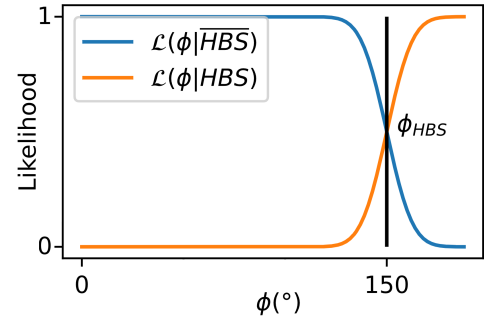

Fig. 4: Algorithm 2: likelihood function for ϕ when human body shadowing is assumed (orange), and when it is not assumed (blue), for a threshold ϕ_{HBS} of $150°$.

and a possible absence of a clear HBS transition as a function of ϕ.

Finally, the weights of each candidate position are normalized and the weighted average position is calculated. This algorithm is labeled as 'LLS-Robustϕ'. Lastly, alternative AS strategies exist which also do not require the CIR or error statistics. [27] is an older method which uses range subsets to calculate candidate positions, and chooses the subset/position with the lowest median of squared range residuals. We implemented this method as a benchmark and labeled it as 'LLS-LMedSq'.

Algorithm 2

Data: n ranges with known anchor positions, tag heading h_{imu}, HBS threshold ϕ_{HBS}
Result: 2D tag position

$WeightedPositions \leftarrow$ list;
$S \leftarrow$ list of all $\sum_{k=3}^{n} \binom{n}{k}$ possible tag-anchor link subsets;
for $S^j \in S$ **do**
    $\mathbf{x}_{tag}^j \leftarrow (2)$ ▷ use links in S^j;
    $\phi^j \leftarrow (1)$ ▷ use$\mathbf{x}_{tag}^j$ and h_{imu}
    $w^j \leftarrow (5);$
    append $w^j \cdot \mathbf{x}_{tag}^j$ to $weightedPositions$;
end for
$\mathbf{x}_{tag} \leftarrow$ sum($WeightedPositions$);

IV. RESULTS

A. Impact of human body orientation on UWB ranging

Figure 5a shows boxplots of the ranging errors in both environments as a function of ϕ in $20°$ intervals. The black box plots represent the errors from the tests in the IIoT lab, which show that the average error remains 0 cm up until $100°$ and the error spread is constant. The 75th and 90th percentile of the absolute errors are 7 cm and 11 cm while true distance is 6 m on average. This conforms to the results measured at 5 m in LOS conditions [24], with the same hardware (settings) and environment. As observed in [5], [20], the human body can therefore be ignored as a source of error in this interval of ϕ. Figure 5 (black) also shows that a positive error bias
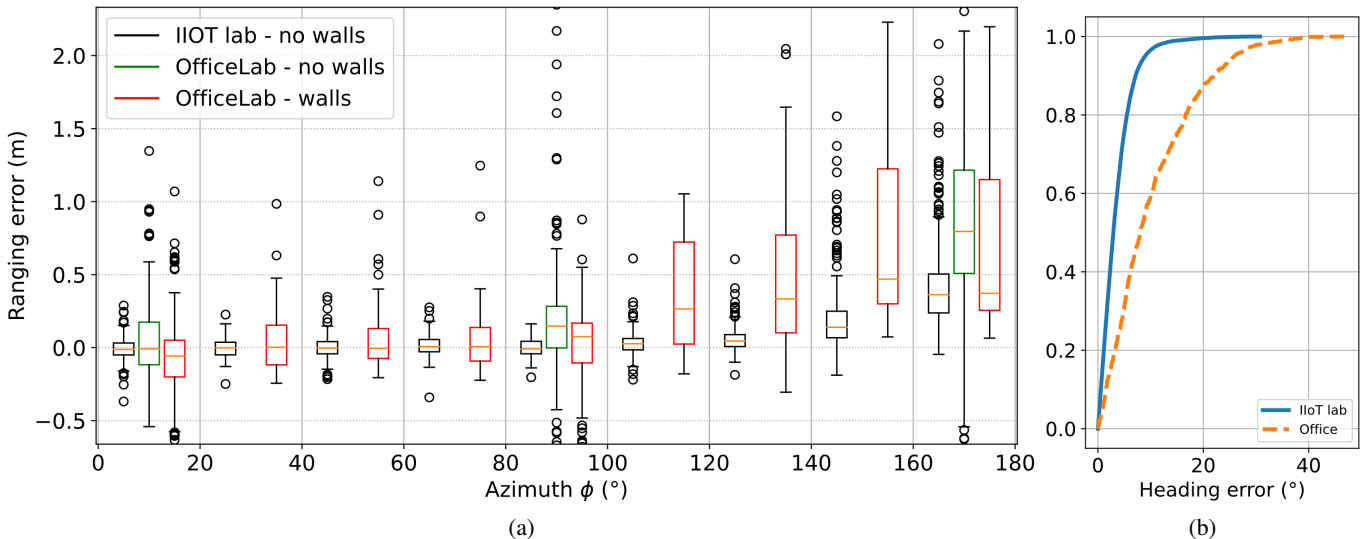
Fig. 5: Boxplots of ranging errors as a function of the ground truth incident angle ϕ in IIoT lab (black), in the office lab with only the human body (green), and with both human body and drywalls as cause of NLOS (red). CDFs of the heading errors of the Adafruit BNO55 IMU in the IIoT lab (blue), and the office lab (orange).

and a larger standard deviation appear for $\phi > 100°$, which both continue to increase with ϕ. More specifically, a positive bias of 4 cm appears for $\phi \in 100° - 140°$ and the 75th and 90th percentile of absolute errors rise to 9 cm ($+29\%$) and 14 cm ($+27\%$). In the $140° - 180°$ interval, the average error is 36 cm and the 75th and 90th percentile of absolute errors are 46 cm ($+557\%$) and 82 cm ($+645\%$), with outliers up to 2.9 m. Note that the exact boundaries differ in other works, which is attributed to the placement and distance of the tag relative to the body.

Furthermore, Figure 5 also shows boxplots of the ranging errors in the office lab. The ranges are split based on the presence of walls between the tag and the anchor. As in the IIoT lab, the signals from anchors located in the corridors (green) do not pass through walls, whereas the signals of anchors outside of the corridor do (red). The former are only represented in three azimuth intervals, because only measurements in the four cardinal directions were performed and the measurement positions and corridor anchors are almost collinear.

Regardless of the location of the anchors, the range errors in office lab follow the same trend as a function of ϕ as in the IIoT lab, but they are more dispersed in every interval. This is expected in a realistic environment, which introduces errors that are independent of the body orientation.

B. Impact of IMU-based mitigation of human body shadowing in UWB positioning

First, the parameters of the various algorithms are discussed. The threshold ϕ_{HBS} has the same value for all orientation-based algorithms, which is the value for which the LLS-ASϕ_{mocap} algorithm has the lowest mean

error. $\phi_{HBS} = 150°$ in the IIoT lab and $\phi_{HBS} = 100°$ in the office lab. These values correspond roughly with the intervals in Figure 5a where the slope of the average range error increases. The LLS-Robustϕ algorithm has a second parameter: the standard deviation of the likelihood functions. We set this value to $5°$ in the IIoT lab and $15°$ in the office environment, which corresponds to the standard deviation of the IMU heading (h_{imu}) error in both environments respectively. Furthermore, Figure 5b shows the CDFs of the absolute errors of h_{imu} in both environments.

The optimal threshold for the LLS-AS_FP algorithm is 15 dB, and the LLS-LMedSq algorithm does not require any parameters. Note that we had to set the minimum amount of anchors from three (IIoT) to four in the office lab to have any improvement compared to the LLS algorithm. This is attributed to the Geometric Dilution of Precision (GDOP), which is higher for measurement positions outside of the polygon formed by the anchors as is the case in the office labe (see Figure 2c), and is inversely proportional to the amount of anchors. Therefore it is better to select at least four range measurements, even if they are affected by HBS.

Figure 6 shows the CDFs of the localization errors of the algorithms discussed in section III in the IIoT lab (a) and the office lab (b). A summary of several error statistics is provided in Table II and Table III respectively. All HBS mitigation algorithms perform well compared to the LLS algorithm, showing an average reduction of 31% and 36% of the median and p75 errors. The orientation-based algorithms perform better on the higher error statistics, with the LLS-Robustϕ and LLS-ASϕ_{mocap} algorithms performing best and almost equally, with a 49%, average of 73% and 68% reduction of the p90, p99, and maximum errors respectively.

The performance of LLS-AS_FP, although slightly lower than the orientation-based algorithms, confirms that the first path power can be used for NLoS/HBS detection and mitigation. LLS-ASϕ_{imu} performs close to its ideal version $LLS - AS\phi_{imu}$ in the IIoT lab, because both the IMU heading and LLS algorithm achieve good results in this environment.

The results in the office lab show our motivation for the robust orientation-based algorithm (LLS-Robustϕ). The accuracy of the LLS algorithm and of the IMU heading have degraded to the extent that the LLS-ASϕ_{imu} algorithm increases the localization error compared to the LLS algorithm. Surprisingly no improvement is shown with the FP-based algorithm either. The LLS-Robustϕ algorithm performs best, followed by the LLS-LMedSq algorithm, showing a 50% and 35% reduction of the average error respectively.

TABLE II: IIoT lab: localization error statistics in m for the algorithms discussed in section III

Algorithm	Localization error (m)					
	mean	p50	p75	p90	p99	max.
LLS	0.26	0.18	0.3	0.51	1.77	2.14
LLS-AS_FP	0.19	0.12	0.19	0.35	1.05	1.25
LLS-ASϕ_{imu}	0.16	0.13	0.19	0.29	0.70	0.77
LLS-ASϕ_{mocap}	0.15	0.12	0.18	0.26	0.52	0.69
LLS-LMedSq	0.19	0.13	0.23	0.43	1.02	1.15
LLS-Robustϕ	0.15	0.12	0.19	0.26	0.45	0.69

TABLE III: Office lab: localization error statistics in m for the algorithms discussed in section III

Algorithm	Localization error (m)					
	mean	p50	p75	p90	p99	max.
LLS	1.4	0.6	1.3	2.1	14	18.3
LLS-AS_FP	1.5	0.6	1.5	2.1	14	18.3
LLS-ASϕ_{imu}	1.7	0.6	1.5	3.6	14	18.3
LLS-ASϕ_{mocap}	1.3	0.5	1.0	1.9	14	18.3
LLS-LMedSq	0.9	0.5	1.2	2.0	3.8	4.4
LLS-Robustϕ	0.7	0.5	0.8	1.4	2.2	2.3

V. CONCLUSIONS AND FUTURE WORK

NLoS detection and mitigation in UWB positioning is a complex problem, which is still a popular topic after two decades of research. This paper focuses on detection and mitigation of human body shadowing, a special case of NLoS in which the body of a pedestrian carrying a tag obstructs the direct path between the tag and one or more anchors. We proposed a mitigation strategy in which an IMU is attached to the UWB tag to estimate the tag heading. An initial/candidate position estimate and the heading are used to estimate the body-tag orientation relative to the anchors, in order to assess the HBS influence. This approach does not require detailed error statistics, but is dependent on the accuracy of candidate position estimates and estimated heading. A robust algorithm was proposed to tackle these dependencies. The algorithm first estimates candidate positions from several anchor subsets and then estimates the relative orientation of these positions
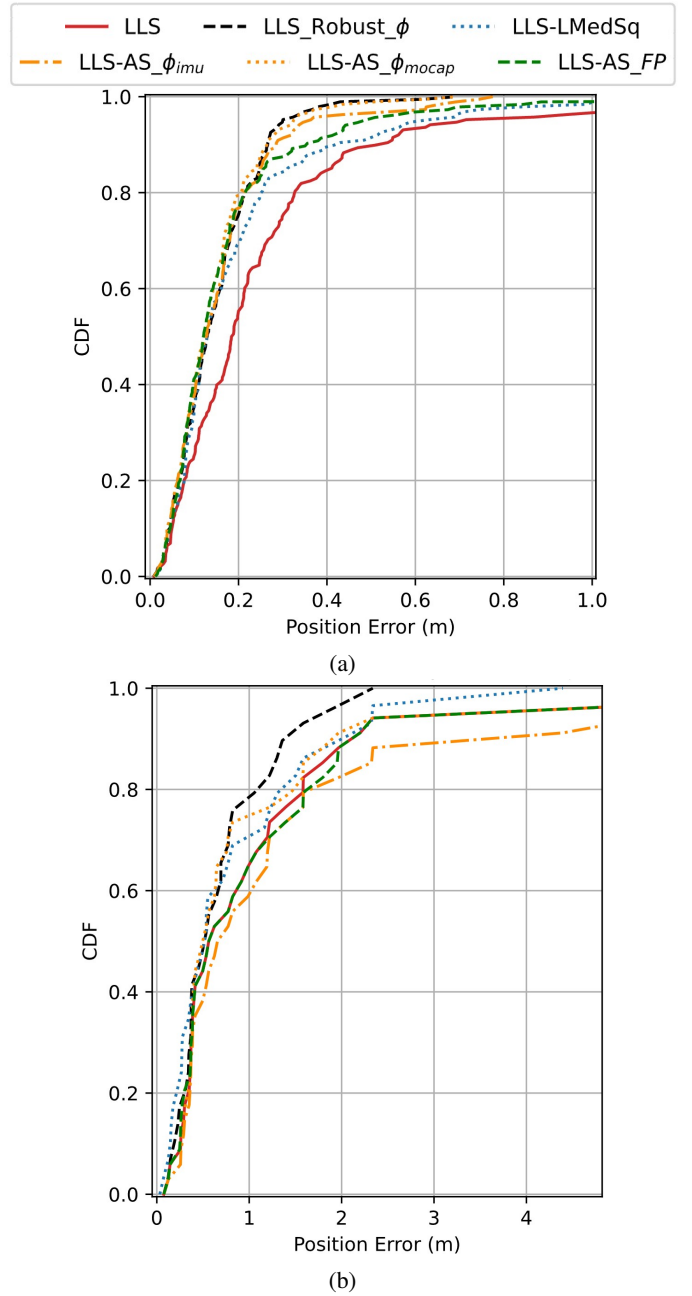

Fig. 6: CDFs of localization errors for the algorithms discussed in section III, in IIoT lab (a) and the office lab (b)

using the IMU heading. The candidate positions are weighted by likelihood functions based on the estimated orientations. The algorithm is validated with measurements in two environments, an IIoT lab and an office lab. It outperforms similar algorithms in the higher error statistics, with a 49% and 33% reduction of the p90 error in the IIoT and office environments respectively. In the future, more extensive experiments will be performed in a variety of realistic environments. Furthermore, the experiments performed for this research were static. Future research will include experiments with a mobile tag.

REFERENCES

[1] Abdulrahman Alarifi, AbdulMalik Al-Salman, Mansour Alsaleh, Ahmad Alnafessah, Suheer Alhadhrami, Mai Al-Ammar, and Hend Al-Khalifa. Ultra wideband indoor positioning technologies: Analysis and recent advances. *Sensors*, 16:1–36, 05 2016.

[2] Antonio Ramon Jimenez Ruiz and Fernando Seco Granja. Comparing Ubisense, BeSpoon, and DecaWave UWB Location Systems: Indoor Performance Analysis. *IEEE Transactions on Instrumentation and Measurement*, 66(8):2106–2117, aug 2017.

[3] Kegen Yu, Kai Wen, Yingbing Li, Shuai Zhang, and Kefei Zhang. A novel NLOS mitigation algorithm for UWB localization in harsh indoor environments. *IEEE Transactions on Vehicular Technology*, 68(1):686–699, 2019.

[4] Timothy Otim, Luis E. Díez, Alfonso Bahillo, Peio Lopez-Iturri, and Francisco Falcone. Effects of the body wearable sensor position on the UWB localization accuracy. *Electronics (Switzerland)*, 8(11):1–14, 2019.

[5] Timothy Otim, Alfonso Bahillo, Luis Enrique Díez, Peio Lopez-Iturri, and Francisco Falcone. FDTD and Empirical Exploration of Human Body and UWB Radiation Interaction on TOF Ranging. *IEEE Antennas and Wireless Propagation Letters*, 18(6):1119–1123, 2019.

[6] Matteo Ridolfi, Stef Vandermeeren, Jense Defraye, Heidi Steendam, Joeri Gerlo, Dirk De Clercq, Jeroen Hoebeke, and Eli De Poorter. Experimental evaluation of uwb indoor positioning for sport postures. *Sensors (Switzerland)*, 18(1):1–20, 2018.

[7] Vitomir Djaja-Josko and Marcin Kolakowski. A new map based method for NLOS mitigation in the UWB indoor localization system. *2017 25th Telecommunications Forum, TELFOR 2017 - Proceedings*, 2017-Janua:1–4, jan 2018.

[8] Qiang Zhang, Dengkang Zhao, Shaojun Zuo, Tingting Zhang, and Dan Ma. A low complexity NLOS error mitigation method in UWB localization. *2015 IEEE/CIC International Conference on Communications in China, ICCC 2015*, pages 0–4, 2016.

[9] Soumya Prakash Rana, Maitreyee Dey, Hafeez Ur Siddiqui, Gianluigi Tiberi, Mohammad Ghavami, and Sandra Dudley. UWB localization employing supervised learning method. *2017 IEEE 17th International Conference on Ubiquitous Wireless Broadband, ICUWB 2017 - Proceedings*, 2018-Janua:1–5, 2018.

[10] Vladimir Savic, Erik G. Larsson, Javier Ferrer-Coll, and Peter Stenumgaard. Kernel Methods for Accurate UWB-Based Ranging with Reduced Complexity. *IEEE Transactions on Wireless Communications*, 15(3):1783–1793, 2016.

[11] Enrique Garcia, Pablo Poudereux, Alvaro Hernandez, Jesus Urena, and David Gualda. A robust UWB indoor positioning system for highly complex environments. *Proceedings of the IEEE International Conference on Industrial Technology*, 2015-June(June):3386–3391, jun 2015.

[12] André G. Ferreira, Duarte Fernandes, André P. Catarino, and João L. Monteiro. Performance Analysis of ToA-Based Positioning Algorithms for Static and Dynamic Targets with Low Ranging Measurements. *Sensors (Basel, Switzerland)*, 17(8), aug 2017.

[13] Laura Flueratoru, Silvan Wehrli, Michele Magno, Elena Simona Lohan, and Dragoş Niculescu. High-accuracy ranging and localization with ultrawideband communications for energy-constrained devices. *IEEE Internet of Things Journal*, 9(10):7463–7480, 2022.

[14] Karthikeyan Gururaj, Anojh Kumaran Rajendra, Yang Song, Choi Look Law, and Guofa Cai. Real-time identification of nlos range measurements for enhanced uwb localization. In *2017 International Conference on Indoor Positioning and Indoor Navigation (IPIN)*, pages 1–7, 2017.

[15] Yan Wang and Xin Li. The imu/uwb fusion positioning algorithm based on a particle filter. *ISPRS International Journal of Geo-Information*, 6, 08 2017.

[16] Alwin Poulose, Jihun Kim, and Dong Seog Han. A sensor fusion framework for indoor localization using smartphone sensors and wi-fi rssi measurements. *Applied Sciences*, 9(20), 2019.

[17] Yuan Wu, Hai Bing Zhu, Qing Xiu Du, and Shu Ming Tang. A Survey of the Research Status of Pedestrian Dead Reckoning Systems Based on Inertial Sensors. *International Journal of Automation and Computing*, 16(1):65–83, 2019.

[18] Eriko Sasaki, Hidenobu Hanaki, Hiroaki Iwashita, Kazuki Naiki, and Akihiro Kajiwara. Effect of human body shadowing on UWB radio channel. *2016 International Workshop on Antenna Technology, iWAT 2016*, pages 68–70, 2016.

[19] Bomono A. Emessiene Thad. B. Welch, Senior Member, IEEE, Randall L. Musselman, Senior Member, IEEE. The Effects of the Human Body on UWB Signal Propagation in an Indoor Environment. *Journal of Electromagnetic Waves and Applications*, 26(4):560–569, 2012.

[20] Qinglin Tian, Kevin I.Kai Wang, and Zoran Salcic. Human body shadowing effect on uwb-based ranging system for pedestrian tracking. *IEEE Transactions on Instrumentation and Measurement*, 68(10):4028–4037, 2019.

[21] Timo Kumpuniemi, Matti Hamalainen, Juha Pekka Makela, and Jari Iinatti. Path loss modeling for UWB creeping waves around human body. *International Symposium on Medical Information and Communication Technology, ISMICT*, pages 44–48, 2017.

[22] Sander Coene, Cedric De Cock, Emmeric Tanghe, David Plets, Luc Martens, and Wout Joseph. Using sage on cots uwb signals for toa estimation and body shadowing effect quantification. In *2021 International Conference on Indoor Positioning and Indoor Navigation (IPIN)*, pages 1–8, 2021.

[23] Timothy Otim, Alfonso Bahillo, Luis Enrique Díez, Peio Lopez-Iturri, and Francisco Falcone. Towards sub-meter level uwb indoor localization using body wearable sensors. *IEEE Access*, 8:178886–178899, 2020.

[24] Ben Van Herbruggen, Bart Jooris, Jen Rossey, Matteo Ridolfi, Nicola Macoir, Quinten Van Den Brande, Sam Lemey, and Eli De Poorter. Wipos: A low-cost, open source ultra-wideband (UWB) hardware platform with long range sub-GHZ backbone. *Sensors (Switzerland)*, 19(7):1–16, 2019.

[25] Nicola Macoir, Jan Bauwens, Bart Jooris, Ben Van Herbruggen, Jen Rossey, Jeroen Hoebeke, and Eli De Poorter. Uwb localization with battery-powered wireless backbone for drone-based inventory management. *Sensors*, 19(3), 2019.

[26] Abdelmoumen Norrdine. An algebraic solution to the multilateration problem. In *2012 International Conference on Indoor Positioning and Indoor Navigation (IPIN)*, 11 2012.

[27] Roberto Casas, Álvaro Marco, Josechu Guerrero, and Jorge Falco. Robust estimator for non-line-of-sight error mitigation in indoor localization. *EURASIP journal on advances in signal processing*, 2006, 12 2006.

[28] Chunxue Chen, Zheng Huang, Jiayu Wang, Lei Yuan, Jun Bao, and Zhuming Chen. Channel-quality-evaluation-based anchor node selection for uwb indoor positioning. *Electronics*, 11(3), 2022.

[29] Qinglin Tian, Kevin I-Kai Wang, and Zoran Salcic. An ins and uwb fusion approach with adaptive ranging error mitigation for pedestrian tracking. *IEEE Sensors Journal*, 20(8):4372–4381, 2020.